Polarization and Dispersion Properties of Elliptical Hole Golden Spiral Photonic Crystal Fiber

Arti Agrawal, N. Kejalakshmy, B. M. A. Rahman and K. T. V. Grattan

School of Engineering and Mathematical Sciences,
City University London, London, EC1V 0HB, United Kingdom.

Corresponding author: b.m.a.rahman@city.ac.uk

Abstract An elliptical air-hole golden spiral photonic crystal fiber (EGS-PCF) is analysed with the full-vectorial finite element method. The air-holes in the EGS-PCF are arranged in a spiral pattern governed by the Golden Ratio, where the design has been inspired by the optimal arrangement of seeds found in nature. The EGS-PCF exhibits extremely high birefringence (~0.022 at operating wavelength 1550*nm*) which is particularly useful for generating a polarization stable supercontinuum (SC). The fiber can also be designed to have a Zero Dispersion Wavelength (ZDW) at a suitable wavelength for only one polarization and large negative dispersion for the other, leading to a single polarization SC. In addition, the fiber dispersion can be designed to obtain ZDWs at 800*nm* and 1064*nm* simultaneously which can facilitate broadband supercontinuum generation (SCG) through multi-wavelength pumping.

1 Introduction

Photonic Crystal Fibers (PCF) that guide light through the mechanism of modified total internal reflection usually have a high index core surrounded by a cladding with a lower average index due to an air-hole microstructure. Large birefringence can be achieved in such PCF due to the large index contrast as well as the potential to tailor the arrangement and shape of the air-holes. Air-holes in the PCF cladding can be arranged in a manner (with suitable hole-to-hole distance and location) to compensate for the material dispersion and obtain anomalous dispersion at wavelengths below the material Zero Dispersion Wavelength (ZDW). Therefore, it is possible to obtain polarization and waveguide dispersion behaviour needed for wide ranging applications. For example, highly birefringent fibers have application in high bit-rate communication systems, gyroscopes, sensing, in fiber lasers with single polarization output and in polarization stable SCG [1-3]. Non-linear PCF with a suitable dispersion have been used for SCG [4] to create sources for optical coherence tomography, frequency metrology and in the case of polarized SCG for tunable/UV generation [5]. Birefringence values of the order of 10^{-2} can be achieved with PCF through exploiting asymmetry of the core or of the cladding (or a combination of both) [6-9]. However, the complicated arrangement of air-holes of different sizes and/or shapes makes fabrication challenging [7-9]. Recently, a highly birefringent PCF design called the Golden Spiral PCF (GS-PCF) [6] was presented, which has large phase birefringence (~0.016 at operating wavelength 1550*nm*, in this paper we refer to the phase modal birefringence as the birefringence). In this letter, the polarization and dispersion properties of the elliptical hole GS-PCF (termed the EGS-PCF) are presented. The fiber birefringence increases by 30% to 0.022 at operating wavelength 1550*nm* and has dispersion that can be tuned for very stable

SCG (without polarization fluctuations), single polarization SCG and even for ultra-broadband SCG.

2 The EGS-PCF structure

In the GS-PCF the air-holes are arranged in a golden spiral pattern that is asymmetric near the core area (see Fig. 1 [6]) and mimics the arrangement of growth of seeds in plants. It represents optimum utilization of space in the sense that it is possible to have large air fill fraction of upto 82.5% even with an irregular arrangement of air-holes (where air fill fraction is defined as the ratio of air-hole radius (r) and the spiral radius for the GS-PCF, r_o). However, in the present case (EGS-PCF) all the identical air-holes are elliptical in shape. The semi-major and minor axes of the elliptical air-holes are denoted by a and b respectively. The larger the ratio a/b greater is the ellipticity ($\varepsilon=a/b$) of the air-hole. For the case where $a=b$, the elliptical air-holes simply become circular (we will denote circular air-hole radius by r). Further, we define the air-hole orientation as horizontal, 'h', when the semi-major axis of the ellipse is along the x direction and vertical, 'v', when it is along the y direction respectively (see Figs. 1 and 2). A full vectorial Finite Element Method (FEM) [10] has been used to compute the birefringence of the EGS-PCF. The number of air-holes is kept constant at 43 in the numerical results reported. The Sellmeier equation has been used to obtain the refractive index of silica at different wavelengths to account for the material dispersion. About 65,000 second order triangular elements, arranged in an irregular mesh with 459617 nodal points, have been used to simulate the EGS-PCF structure using the COMSOL software. A single simulation run on a 64 bit quad-core Intel Pentium desk top computer took about 100s.

3 Birefringence Properties of the EGS-PCF

We examine the effect of changing air-hole shape from circular to elliptical on the birefringence while air-hole area is kept constant. Figure 3 shows the absolute value of birefringence as a function of wavelength for the two orientations. The solid curve represents the birefringence for the PCF with circular air-holes (r/r_o=0.70, r_o=0.45μm, r=0.315 μm). Elliptical air-holes of the same area as the circular air-holes are formed by stretching the circular air-holes in the x(y) direction and squeezing by the same amount in the y(x) direction. The curves with the triangular and square symbols represent elliptical air-holes in the 'h' and 'v' orientations respectively. We first look at the 'h' orientation and note that as the air-holes become more elliptical the birefringence increases substantially relative to circular air-holes. The y polarized mode for the elliptical air-hole PCF in the 'h' orientation has a lower effective index than the corresponding circular air-hole PCF (see Figs. 4a and 4b), as the high index silica regions in between air-holes which the field can enter are larger in the latter design. On the other hand, the effective index of the x polarized mode in the 'h' orientation is larger than that of the corresponding x polarized mode for the circular air-hole PCF, since the electric field spreads more in the x direction in silica in the former case due to the elongation(squeezing) of air-holes in x(y) direction and enhancement of the structural asymmetry. Since the effective index difference between the two modes is enhanced in the 'h' orientation, the birefringence is larger.

In the 'v' orientation, the effective index of the y polarized mode is larger than the x polarized mode of the same structure because the air-holes block spreading of the field into high index silica regions more in the x direction than in the y direction. Also n_{eff} for the y polarized mode is lower than the corresponding y polarized mode in the circular air-hole PCF at lower ellipticity (see Fig. 4c), while it is higher with increase in ellipticity (see fig. 4d). This occurs because in the former case, as the field spreads in the y-direction it encounters longer air-holes and effectively sees a larger air volume. However, with increase in ellipticity, the air-holes become very narrow and a larger proportion of the field can escape into the large

index silica regions leading to larger effective index relative to the circular air-holes (see Fig. 4d) The effective index of the *x* polarized mode is also lower than the circular air-hole PCF (for $a=1.1r$, $b=r/1.1$), see Fig. 4c, since the electric field spread into silica in the *x* direction is blocked more effectively by the elliptical air-holes than the circular air-holes. As the difference between the effective indices of both the polarizations is reduced in the 'v' orientation, the birefringence is lower. The curve for 'v' orientation where $a=1.2r$, $b=r/1.2$, does cross the circular air-hole birefringence at about $1.73\mu m$ since the effective index for the *y* polarized mode increases and is higher than that of the corresponding circular air-hole case as discussed above while the air-hole orientation continues to suppress the effective index for the *x*-polarized mode. We conclude from these results that keeping air-hole area constant (and therefore the air-filling fraction) birefringence increases with the ellipticity of air-holes oriented in a manner that enhances the structural asymmetry seen by the field.

We next examine the effect of increasing the ellipticity of air-holes for designs with larger air fill fractions in the 'h' and 'v' orientations where air-hole area maybe lower than that of circular air-holes. Figure 5 shows the absolute value of birefringence (for $r/r_o=0.80$, $r_o=0.45\mu m$, $r=0.36\mu m$) as a function of wavelength for circular and elliptical air-holes; where the semi-major axis of the elliptical air-holes $a=r$, but the semi-minor, b is smaller, resulting in elliptical air-holes with lower area than the circular air-holes. We first note that comparing the birefringence of circular air-holes in Figs. 3 and 5 shows that larger air-fill fraction yields larger birefringence (since the core-cladding index difference is enhanced), which is in agreement with previous results [6]. From Fig. 5 it can also be seen that for shorter wavelengths, the circular air-hole design has a slightly larger birefringence, but as the wavelength increases the birefringence is much larger with elliptical air-holes, especially in the 'h' orientation. In the 'h' orientation the effective index of the *x* polarized mode increases as the field can spread more easily into silica in the *x* direction (and as the air-holes become narrower with increasing ellipticity, the effective index increases) while the *y* polarized mode sees needle shaped air-holes that block the field spreading in silica in the *y* direction. This enhances the birefringence even though the air filling fraction is lower than the circular air-hole PCF.

In the 'v' orientation, for shorter wavelengths, the *y* polarized mode sees long air-holes and consequently the effective index is lowered (similar to the case in Fig. 3). However, as the wavelength increases, the *y* polarized field spreads in the silica regions between air-holes which causes the effective index to increase while the *x* polarized mode is still blocked from spreading too much in silica. This leads to the increase in birefringence for 'v' orientation. The index difference between core and cladding is larger for the circular air-hole PCF, and increase in the spotsize with wavelength leads to the field interacting with a larger number of air-holes for which the arrangement is more symmetric: hence the birefringence saturates or even decreases [6]. While for the EGS-PCF even at longer wavelengths, the asymmetry of the field distribution in the cladding contributes to increase in the birefringence. At $1550nm$ the largest birefringence is 0.02 (for $r/r_o=0.80$).

Figure 6 shows the effect of the air-hole ellipticity on the birefringence variation with wavelength for both orientations (for $r/r_o=0.825$, $r_o=0.45\mu m$, $r=0.3712\mu m$). Similar to Fig.5 it can be noted that birefringence increases with ε. For all values of ε the birefringence is larger for the 'h' orientation, especially for the case $a=r$, $b=r/3$. The physical mechanism is similar to that responsible for the birefringence variation in Fig. 5, and the larger r/r_o fraction yields larger birefringence values. The largest value obtained is 0.022 at $1550nm$ (in 'h' orientation, $a=r$, $b=r/3$, core diameter~$1\mu m$ and A_{eff} ~$7\ \mu m^2$) while for an extremely well confined field, a birefringence value as large as 0.018 (in 'h' orientation, $a=r$, $b=r/2$, core diameter~$1\mu m$ and A_{eff} ~$4\ \mu m^2$) is obtained. An increase in ε is accompanied by a decrease in the air volume: therefore, the field is less well confined and for extremely large ellipticity where the air-holes

are barely open slits, both the orthogonally polarized modes see similar air filling fraction (in both orientations) and birefringence saturates to similar values for both orientations.

Further more, we mention here that the absolute value of the group modal birefringence (which is linked to the first derivative of the phase birefringence) of the EGS-PCF at 1550nm is of the order of 10^{-2}-10^{-3}.

Thus, the ellipticity provides an additional way to control the birefringence as well as the degree of mode confinement (hence dispersion) in the PCF.

4 Dispersion Properties of the EGS-PCF

An important aspect of the highly birefringent PCF is the difference in the dispersion properties of the two orthogonal polarizations [6]. This property can be exploited to generate ultra-broadband SCG or suppress Stimulated Raman Scattering (SRS) for flat SCG through multi-wavelength pumping [11]. When the two orthogonally polarized PCF modes have different ZDWs, the total SC output is a linear combination of the two continua generated by pumping the SCG for the two modes [1]. With the EGS-PCF it is possible to tune the ZDWs such that one mode has small anomalous dispersion while the other has normal dispersion for single polarization SCG; for the ZDWs of the two orthogonally polarized modes to lie at different wavelengths, for example, close to 800*nm* and 1064*nm* and this could result in broadband and stable SCG. We compute the total group velocity dispersion of the EGS-PCF using the relation:

$$D = -\frac{\lambda}{c}\frac{d^2 n_{eff}}{d\lambda^2} \qquad (1)$$

and by taking into account the material dispersion of silica as well.

We examine the effect of changing air-hole shape on the dispersion properties while air-hole area and air fill fraction are kept constant. Figures 7a and 7b show the dispersion variation of the EGS-PCF with wavelength for different values of ε (r/r_o=0.70, r_o=0.45μm, r=0.315 μm) while air-hole area is kept constant for the x and y polarized modes in the 'h' orientation respectively. We observe that for x polarized mode as the air-holes become more elliptical the dispersion becomes larger; the first ZDW is blue shifted and the second ZDW is red shifted while the dispersion properties of the y polarized mode do not change as much. For the x polarized modes, as the air-holes become more elliptical they allow the field to spread more in the x direction than circular or vertically oriented elliptical air-holes. Therefore the change in effective index of the x polarized mode is larger and dispersion is steeper than the circular air-hole case. The field interacts with the air-holes near the core at relatively shorter wavelengths and hence the first ZDW gets blue shifted. Also, the long wavelength behaviour (and the second ZDW) is red shifted because the field experiences a lower refractive index in the cladding at longer wavelengths due to the squeezed and elongated air-holes. However, the y polarized mode tends to spread more in the vertical direction and increase in ellipticity of the air-hole does not affect the field as much, hence the dispersion remains largely unaffected. Figures 8a and 8b show the dispersion variation with wavelength in the 'v' orientation. The x polarized mode experiences smaller dispersion change with change in ellipticity than the y polarized mode. The air-holes are elongated more and more (with increasing ε) in the vertical direction and affect the fields spreading in silica in the y direction more than they do the spread in the x direction.

We now present results for dispersion variation with wavelength as air-holes are made more elliptical and air-hole area maybe smaller than that of circular air holes. Figures 9a and 9b show the dispersion variation of the EGS-PCF with wavelength as a function of ε (r/r_o=0.80, r_o=0.45μm, r=0.36 μm) for the x and y polarized modes in the 'h' orientation respectively. As the ellipticity increases (the air-fill fraction decreases) the dispersion for both the polarizations decreases (relative to the circular air-holes) at shorter wavelengths, while it

increases at longer wavelengths. Due to smaller air volume (with increasing ellipticity) the dispersion approaches the material dispersion of silica. For the case of elliptical air-holes with *a=r, b=r/2* we obtain normal dispersion for the *x* polarization while the *y* polarized mode has flat, low anomalous dispersion (see also Fig. 10, *a=r, b=r/3*). This could be extremely useful for generating single polarization SCG.

From the earlier work [Fig. 5 in 6] we know that for a fixed r/r_o ratio as the spiral radius, r_o, is increased, the dispersion becomes lower, flatter and the ZDWs are red shifted. Furthermore it is possible to choose the spiral parameters such that the ZDWs lie close to more than one pump wavelength simultaneously at which commercial sources are available. This can facilitate broadband supercontinuum generation (SCG) through multi-wavelength pumping. For example, for the case *a=r, b=r/2* (Fig. 10), the first ZDW for the *y* polarization lies at 800*nm* while the *x* polarization has the second ZDW at 1064*nm*. Figure 10 shows the dispersion variation of the EGS-PCF with wavelength as a function of ε (r/r_o=0.80, r_o=0.625μm, r=0.5 μm) in the 'v' orientation. As the ellipticity increases (air-fill fraction decreases), the first ZDWs of the dispersion curves for both modes become red shifted while the second ZDWs are blue shifted and the dispersion slope also decreases. A significant point is that the separation between the second ZDWs of the two orthogonal polarizations increases with ε. With the increase in ε, due to smaller air-volume the core-cladding index is smaller and the effective index change (hence dispersion) is less steep. The effective index change with wavelength is relatively more significant at slightly longer wavelengths where the field interacts substantially with the air-holes, hence the red shift in the first ZDW. At longer wavelengths (~1μm and higher), due to the lower air volume in the PCF and the larger spotsizes, the field starts to interact with the outer air-holes at smaller wavelengths and the long wavelength behaviour is blue shifted.

From Fig. 10 we note that for the case where *a=r/2, b=r*, the *y* polarized mode has a ZDW at 800*nm* while the *x* polarized has a ZDW at 1064*nm* and this could result in broadband and stable SCG by multi-wavelength pumping. In Fig. 11 we present the effective modal area for the two polarizations as a function of wavelength (dispersion curves contain triangular symbols, while curves without symbols represent the effective area). It can be seen that the guided modes in both the polarizations have effective areas that are close in value, and since modal area is an indicator of the degree of modal confinement, the two polarizations exhibit similar confinement in the wavelength range of interest (~800-1064*nm*). Thus the air-hole ellipticity provides an additional parameter with which to control the dispersion.

5 Conclusion

In conclusion, the polarization properties of the elliptical hole golden spiral PCF have been presented. The work has shown that the ellipticity of the air-holes can increase the birefringence to 0.022 at 1550*nm*. The dispersion of the highly birefringent EGS-PCF can be most useful in generating a very flat and stable supercontinuum with the suppression of polarization fluctuations and SRS. The fiber can be designed to have a ZDW for only one mode near a pump wavelength and a large negative dispersion for the other mode for single polarization SCG. Furthermore, to generate broadband SCG by multi-wavelength pumping, the ZDWs of the fiber can be made to lie at convenient wavelength locations, such as 800*nm* and 1064*nm* where compact, cost effective and efficient laser sources are commercially available.

References

1. M. Lehtonen, G. Genty, H. Ludvigen and M. Kaivola, "Supercontinuum generation in a highly birefringent microstructured fiber," Appl. Phys. Lett., **82**, 2197 (2003).
2. Z. Zhu and T. G. Brown, "Experimental studies of polarization properties of supercontinua generated in a birefringent photonic crystal fiber," Opt. Express, **12**, 791 (2004).
3. Z. Zhu and T. G. Brown, "Polarization properties of supercontinua generated in birefringent photonic crystal fibers," J. Opt. Soc. Am. B, **21**, 249 (2004).
4. J. M. Dudley, G. Genty and S. Coen, "Supercontinuum generation in photonic crystal fiber," Rev. Mod. Phys. **78**, 1135 (2006).
5. C. Xiong and W. J. Wadsworth, "Polarized supercontinuum in birefringent photonic crystal fiber pumped at 1064nm and application to tuneable/UV generation," Opt. Express, **16**, 2438 (2008).
6. A. Agrawal, N. Kejalakhmy, J. Chen, B.M.A. Rahman and K.T.V. Grattan, "Golden spiral photonic crystal fiber: polarization and dispersion properties," Opt. Lett., **33**, 2716 (2008).
7. K. Suzuki, H. Kubota, S. Kawanishi, M. Tanaka, and M. Fujita, "Optical properties of a low-loss polarization-maintaining photonic crystal fiber," Opt. Express **9**, 676 (2001).
8. D. Chen and L. Shen, "Ultrahigh birefringent photonic crystal fiber with ultralow confinement loss," IEEE Photonics Technol. Lett. **19**, 185 (2007).
9. D. Chen and L. Shen, "Highly birefringent elliptical-hole photonic crystal fibers with double defect," J. Lightwav. Technol. **25**, 2700 (2007).
10. N. Kejalakshmy, B. M. A. Rahman, A. Agrawal, T. Wongcharoen and K. T. V. Grattan, "Characterization of single-polarization single-mode photonic crystal fiber using full-vectorial finite element method," App. Phys. B, **93**, 223 (2008).
11. P-A Champert, V. Couderc, P. Leproux, S. Fevrier, V. Tombelaine, L. Labonte, P. Roy, C. Froehly and P. Nerin, "White-light supercontinuum generation in normally dispersive optical fiber using original multi-wavelength pumping system," Opt. Express, **12**, 4366 (2004).

List of Figures

Figures
Fig. 1

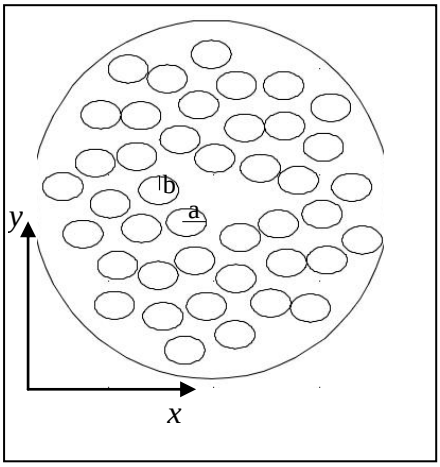

Fig. 2

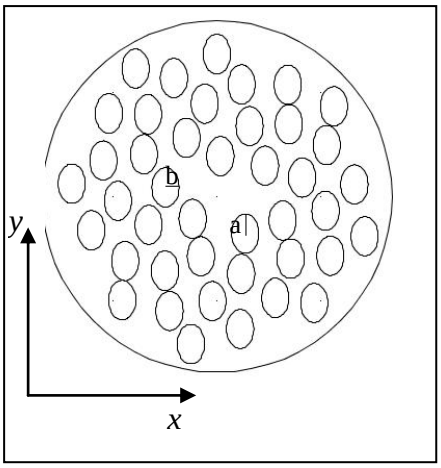

Fig. 3

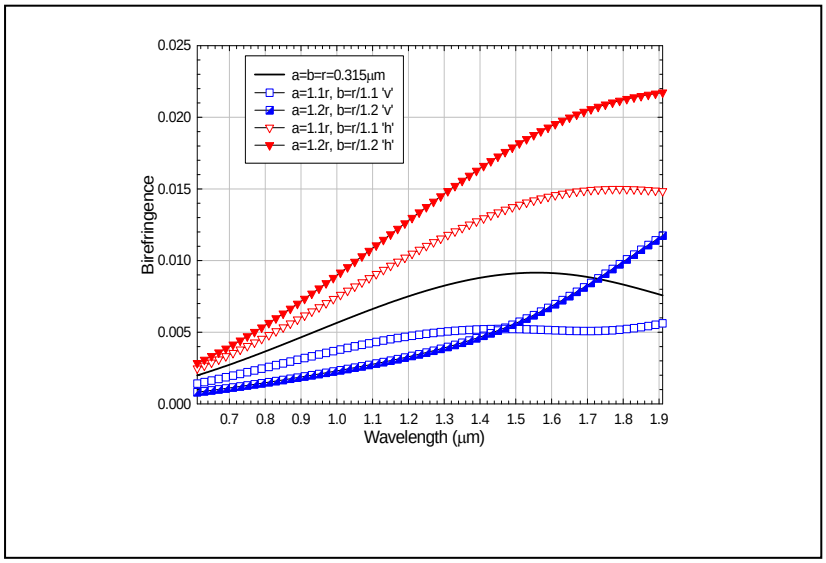
a=b=r=0.315μm
a=1.1r, b=r/1.1 'v'
a=1.2r, b=r/1.2 'v'
a=1.1r, b=r/1.1 'h'
a=1.2r, b=r/1.2 'h'
Birefringence
0.025
0.020
0.015
0.010
0.005
0.000
0.7
0.8
0.9
1.0
1.1
1.2
1.3
1.4
1.5
1.6
1.7
1.8
1.9
Wavelength (μm)

Figs. 4a-d

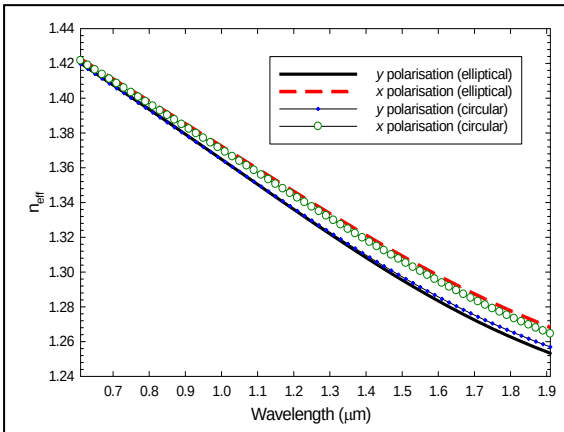

Fig. 4a ‘h’ orientation, *a=1.1r*, *b=r/1.1*

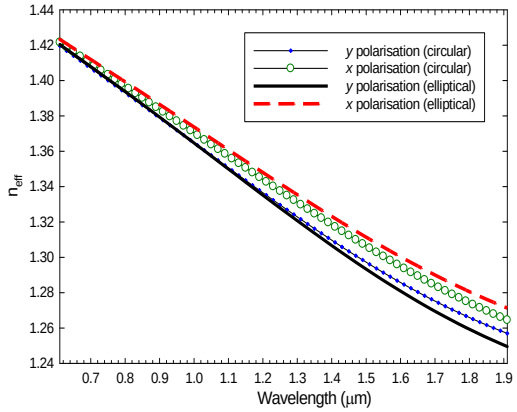

Fig. 4b ‘h’ orientation, *a=1.2r*, *b=r/1.2*

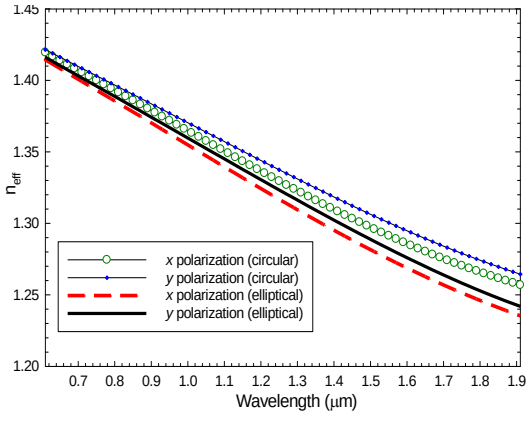

Fig. 4c ‘v’ orientation, *a=r/1.1*, *b=1.1r*

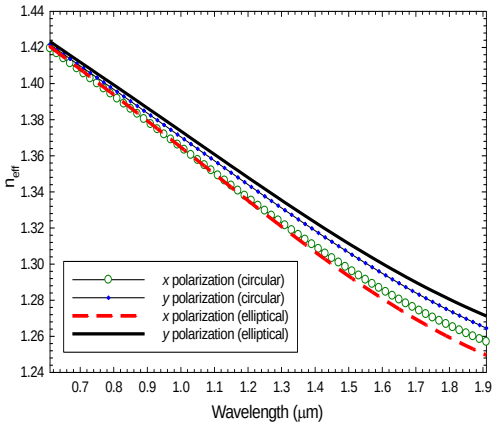

Fig. 4d ‘v’ orientation, *a=r/1.2*, *b=1.2r*

Fig. 5

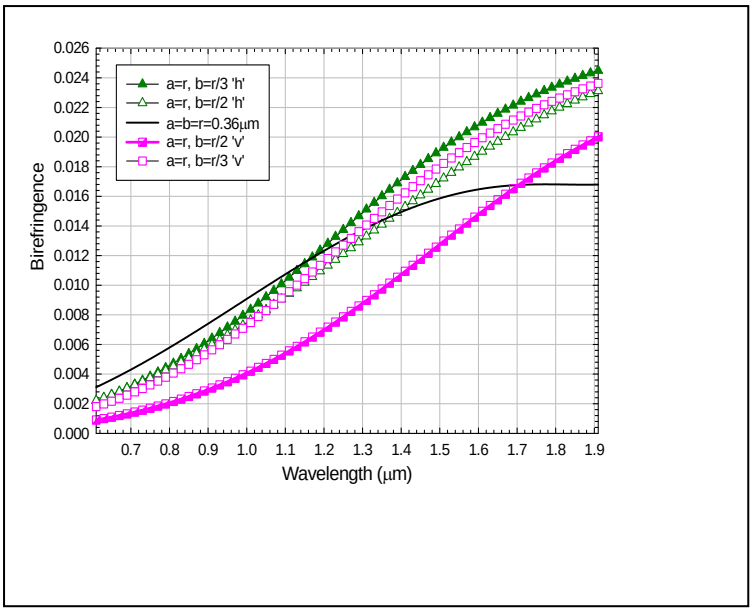
a=r, b=r/3 'h'
a=r, b=r/2 'h'
a=b=r=0.36μm
a=r, b=r/2 'v'
a=r, b=r/3 'v'
Birefringence
0.026
0.024
0.022
0.020
0.018
0.016
0.014
0.012
0.010
0.008
0.006
0.004
0.002
0.000
0.7
0.8
0.9
1.0
1.1
1.2
1.3
1.4
1.5
1.6
1.7
1.8
1.9
Wavelength (μm)

Fig. 6

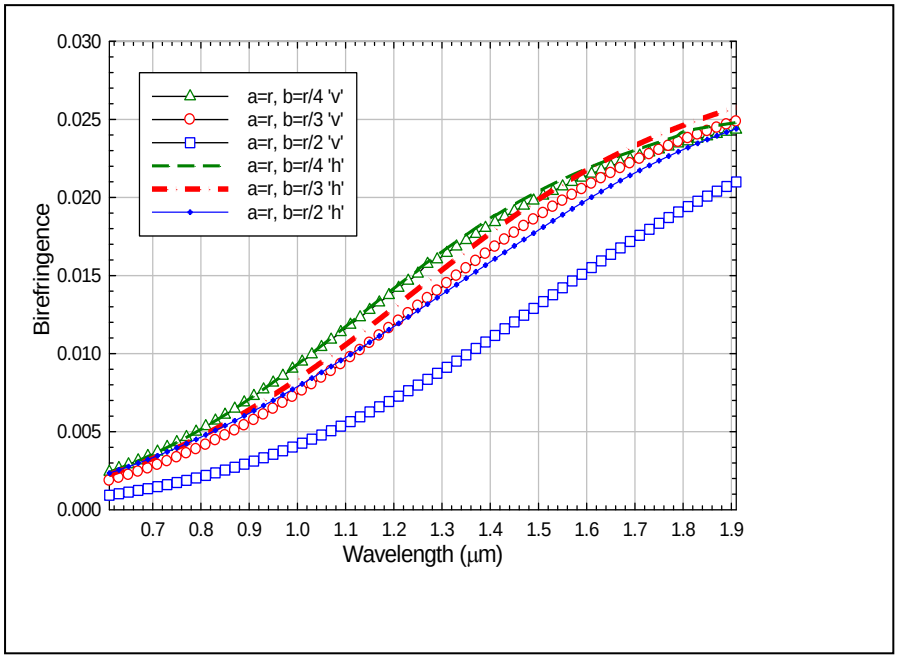
a=r, b=r/4 'v'
a=r, b=r/3 'v'
a=r, b=r/2 'v'
a=r, b=r/4 'h'
a=r, b=r/3 'h'
a=r, b=r/2 'h'
Birefringence
0.030
0.025
0.020
0.015
0.010
0.005
0.000
0.7
0.8
0.9
1.0
1.1
1.2
1.3
1.4
1.5
1.6
1.7
1.8
1.9
Wavelength (μm)

Fig. 7a

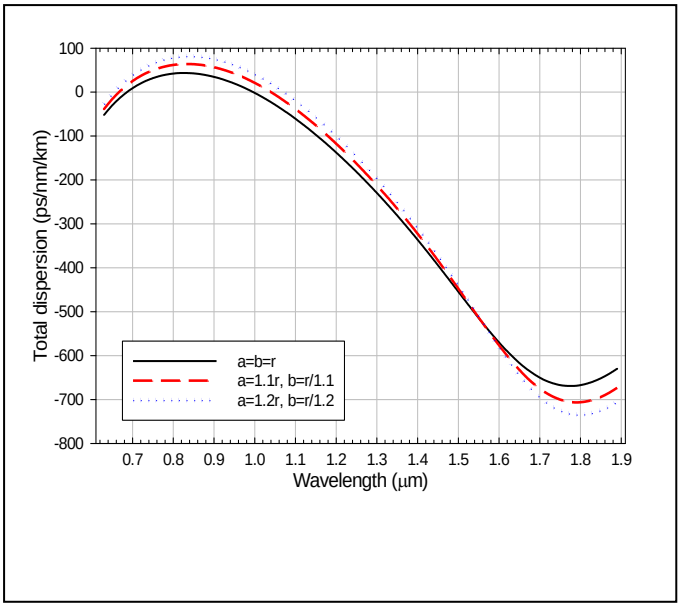
Total dispersion (ps/nm/km)
Wavelength (μm)
a=b=r
a=1.1r, b=r/1.1
a=1.2r, b=r/1.2
100
0
-100
-200
-300
-400
-500
-600
-700
-800
0.7
0.8
0.9
1.0
1.1
1.2
1.3
1.4
1.5
1.6
1.7
1.8
1.9

Fig. 7b

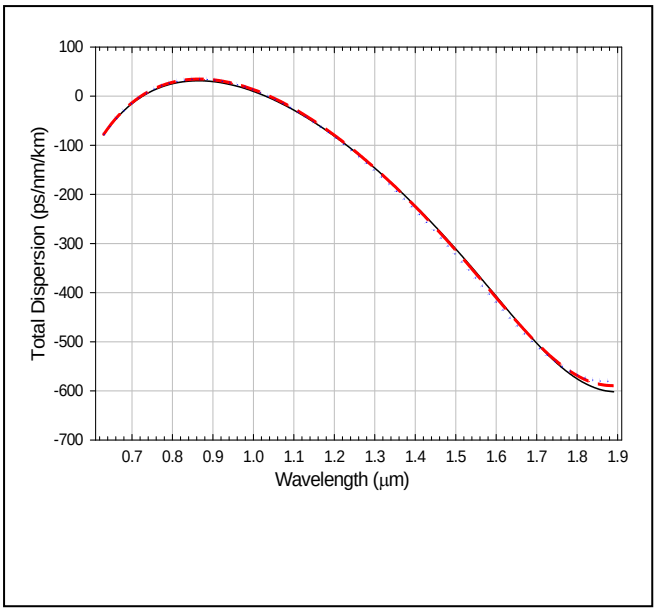
100
0
-100
-200
-300
-400
-500
-600
-700
Total Dispersion (ps/nm/km)
0.7
0.8
0.9
1.0
1.1
1.2
1.3
1.4
1.5
1.6
1.7
1.8
1.9
Wavelength (μm)

Fig. 8a

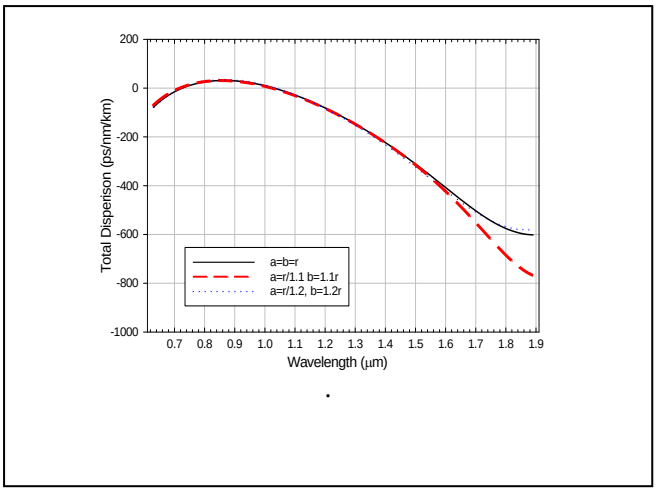
Total Dispersion (ps/nm/km)
200
0
-200
-400
-600
-800
-1000
0.7
0.8
0.9
1.0
1.1
1.2
1.3
1.4
1.5
1.6
1.7
1.8
1.9
Wavelength (μm)
a=b=r
a=r/1.1 b=1.1r
a=r/1.2, b=1.2r

Fig. 8b

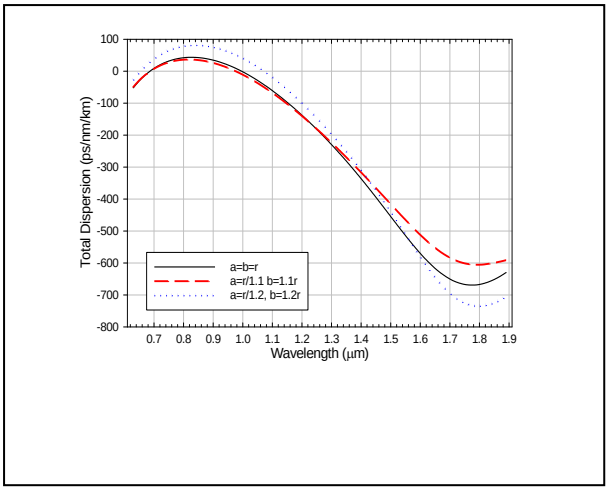
Total Dispersion (ps/nm/km)
Wavelength (μm)
a=b=r
a=r/1.1 b=1.1r
a=r/1.2, b=1.2r

Fig. 9a

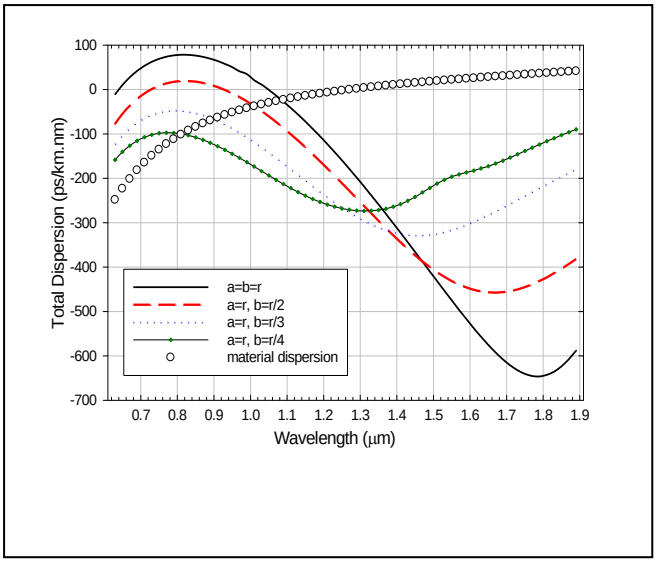
Total Dispersion (ps/km.nm)
Wavelength (μm)
100
0
-100
-200
-300
-400
-500
-600
-700
0.7
0.8
0.9
1.0
1.1
1.2
1.3
1.4
1.5
1.6
1.7
1.8
1.9
a=b=r
a=r, b=r/2
a=r, b=r/3
a=r, b=r/4
material dispersion

Fig. 9b

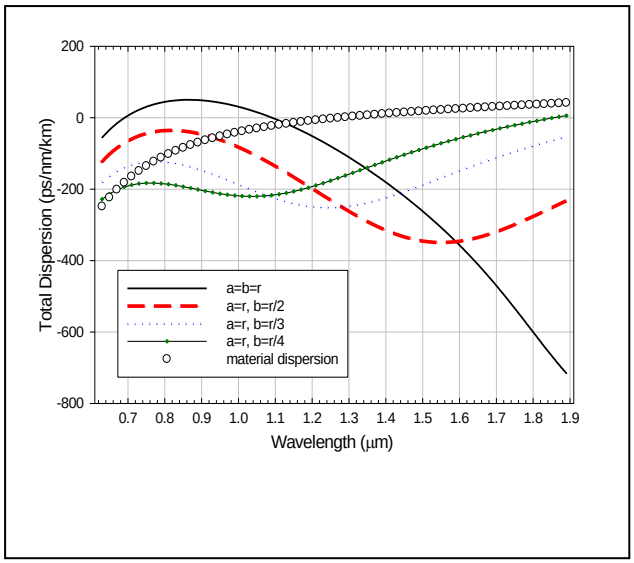
Total Dispersion (ps/nm/km)
Wavelength (μm)
200
0
-200
-400
-600
-800
0.7
0.8
0.9
1.0
1.1
1.2
1.3
1.4
1.5
1.6
1.7
1.8
1.9
a=b=r
a=r, b=r/2
a=r, b=r/3
a=r, b=r/4
material dispersion

Fig. 10

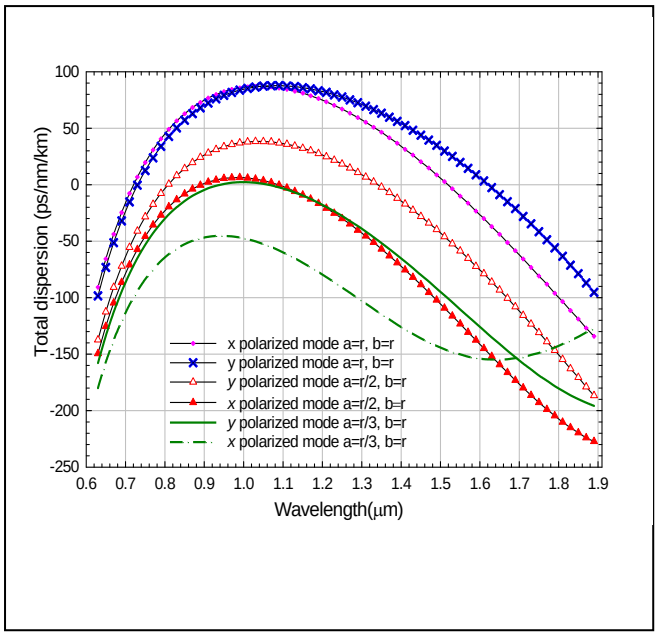
Total dispersion (ps/nm/km)
Wavelength(μm)
100
50
0
-50
-100
-150
-200
-250
0.6
0.7
0.8
0.9
1.0
1.1
1.2
1.3
1.4
1.5
1.6
1.7
1.8
1.9
x polarized mode a=r, b=r
y polarized mode a=r, b=r
y polarized mode a=r/2, b=r
x polarized mode a=r/2, b=r
y polarized mode a=r/3, b=r
x polarized mode a=r/3, b=r

Fig. 11

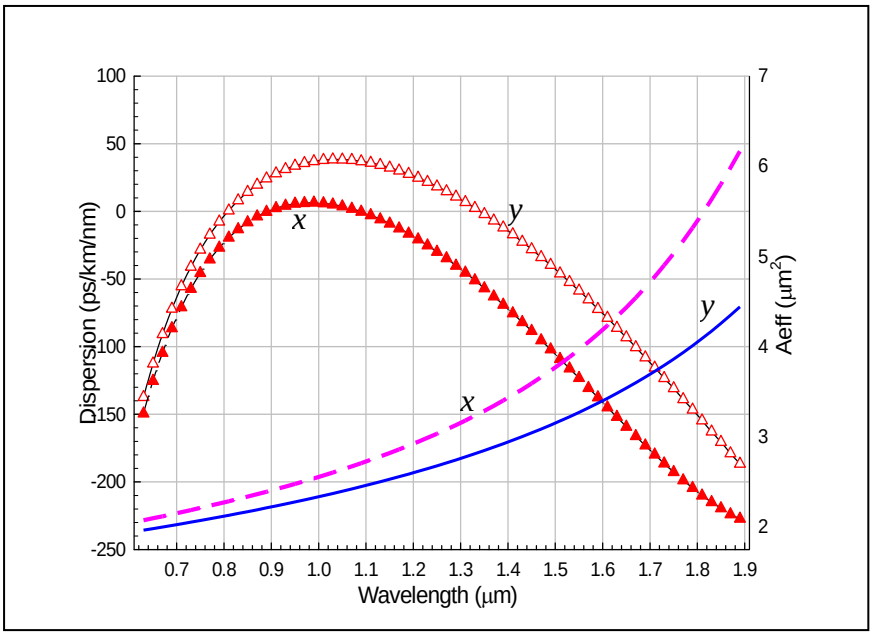
100
50
0
-50
-100
-150
-200
-250
Dispersion (ps/km/nm)
7
6
5
4
3
2
Aeff (μm²)
0.7
0.8
0.9
1.0
1.1
1.2
1.3
1.4
1.5
1.6
1.7
1.8
1.9
Wavelength (μm)
x
y
y
x